Pergamon

Int. J. Solids Structures Vol. 33, No. 1, pp. 33–47, 1996
Copyright © 1995 Elsevier Science Ltd
Printed in Great Britain. All rights reserved
0020-7683/96 $9.50 + .00

0020-7683(95)00023-2

A FINITE ELEMENT APPROACH TO THREE-DIMENSIONAL SINGULAR STRESS STATES IN ANISOTROPIC MULTI-MATERIAL WEDGES AND JUNCTIONS

STEPHANE S. PAGEAU

Department of Mechanical Engineering, Clemson University, Clemson, SC 29634, U.S.A.

and

SHERRILL B. BIGGERS, JR†

Department of Mechanical Engineering Clemson University, Clemson, SC 29634, U.S.A.

(*Received* 15 *July* 1994; *in revised form* 3 *January* 1995)

Abstract – A finite element formulation is developed to determine the order and angular variation of singular stress states due to material and geometric discontinuities in anisotropic materials. The formulation applies to any two-dimensional geometry that is prismatic in the third direction and has three-dimensional displacement fields. In some special cases the three-dimensional fields become uncoupled antiplane and inplane fields and this formulation yields the uncoupled results. The formulation provides for the determination of the asymptotic stress and displacement fields present at interior singular points of three-dimensional structures. The displacement field of the sectorial finite element is quadratic in the angular coordinate direction and asymptotic in the radial direction measured from the singular point. The formulation of Yamada and Okumura [(1983) *Hybrid and Mixed Finite Element Methods*, pp. 325–343. Wiley, Chichester] for inplane problems is adapted for this purpose. The simplicity and accuracy of the formulation are demonstrated by comparison with several analytical solutions for both isotropic and anisotropic multi-material wedges and junctions. The nature and speed of convergence associated with the element suggests that it could be employed in developing two-dimensional and three-dimensional enriched elements for use along with standard elements to yield accurate and computationally efficient solutions to problems having complex global geometries leading to singular stress states.

INTRODUCTION

For two-dimensional problems defined in the x–y plane, i.e. with geometry and external loading invariant in the direction normal to the x–y plane as shown in Fig. 1, Lekhnitskii

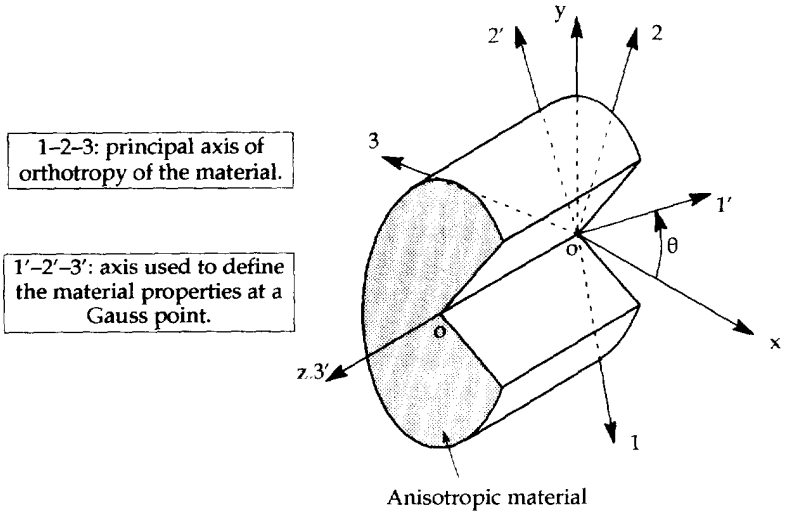

Fig. 1. Geometry of a typical structure in which a singular stress state occurs and reference axis system for determining local mechanical properties.

† Author to whom correspondence should be addressed.

(1963), and Eshelby *et al.* (1953) have developed two equivalent complex-variable formulations which have been used to solve numerous problems of anisotropic elasticity. At about the same time, Stroh (1962) developed a third formulation equivalent to the first two, but more versatile because it does not break down for certain specific cases of orthotropic or isotropic materials. More detailed information concerning the three formulations and their relations to one another can be found in a paper by Suo (1990), specifically in his Section 2 where the basic equations of Stroh's formulation are given and compared with others.

These formulations have been used to find the order of stress singularities and analytical stress and displacement field expressions for prismatic two-dimensional geometries having three-dimensional displacements where a singular stress state exists. Ting and Hoang (1984), Zwiers *et al.* (1982) and Delale (1984) are among the authors of papers which treat these geometries. The materials considered in these papers are anisotropic, i.e. the inplane and antiplane displacement fields are coupled, even though the geometry is two-dimensional in the x–y plane. For such geometries, Ting and Hoang (1984) have shown that pure extensional loading in the z-direction (see Fig. 1) leads to at most a logarithmic singular stress state. As a result, power singularities can be found from considering the same geometry in a state of "generalized" plane strain to simplify the analysis. Here we define generalized plane strain as did Delale (1984), i.e. a plane strain state plus shear strains in the direction normal to the plane. Power singularities obtained under conditions of generalized plane strain do not differ from those obtained in the general three-dimensional case as long as the power singularities calculated lead to a singular stress state. In other words, if stresses are found to be proportional to $r^{\lambda-1}$, the conclusion of Ting and Hoang (1984) holds for values of λ such as $0 < \mathrm{Re}(\lambda) < 1$. The orders of the stress singularities have been obtained previously for some simple geometries and material combinations. To the authors' knowledge, geometries with more than two anisotropic materials have not been considered previously using Stroh's formulation. Indeed, the analytical formulations developed for such geometries are efficient but require rigor in their use. Also, obtaining the angular variation of the displacement and stress fields as well as the orders of stress singularities for geometries containing more than two materials would be quite a lengthy process.

Therefore, the present paper proposes a simple numerical approach to Stroh's (1962) formulation in order to characterize the complete displacement and stress fields for prismatic two-dimensional geometries with three-dimensional displacements. The inplane formulation developed by Yamada and Okumura (1983) is adapted to allow for three-dimensional deformation of two-dimensional wedges and junctions composed of anisotropic materials. The current paper also follows naturally from the papers by Pageau *et al.* (1995a,b) in which two-dimensional wedges and junctions composed of anisotropic materials subject to antiplane shear or inplane loads, respectively, were considered. In other words, these earlier papers considered only one-dimensional or two-dimensional deformation of two-dimensional structures whereas the current paper considers three-dimensional deformations.

The current formulation uses the conclusion of Ting and Hoang (1984) regarding singularities due to z-direction extension. Therefore, generalized plane strain is considered here, although the numerical results that are obtained would have been identical if the generalized plane strain constraint had not been imposed. Therefore, only power singularities are of interest in this paper and logarithmic singularities resulting from extension normal to the plane defined by the multi-material wedges and junctions are disregarded. A recent paper by Pageau and Biggers (1995c) has investigated singular stress states at free edges using a general three-dimensional approach. The formulation of that paper can also be used for the geometries considered here, although it is far more computationally expensive than the current approach. Since the general three-dimensional formulation does not make use of the generalized plane strain assumption, it is used here as a check on all results obtained using the current approach, and also as a validation of the conclusion of Ting and Hoang (1984). The formulation is also verified by comparison with existing analytical solutions by Ting and Hoang (1984) and Delale (1984). Finally, the method is extended to typical multi-material junctions in which singular stress states are present due to material and geometrical discontinuities. Results for both the order of the stress singularities and

the angular variation of the displacement are presented. These examples demonstrate the simplicity and accuracy of the method.

FORMULATION

Figure 1 presents a typical prismatic two-dimensional geometry where a singular stress state occurs at points along the line o–o. This formulation presents a finite element method to determine the order of the stress singularity at a typical point along the line o–o away from external boundaries. For this purpose, the geometry is divided into a number of quadratic sectorial elements, with each element being located in polar coordinates by its nodes 1, 2 and 3 as shown in Fig. 2. A point P in the element can be located using the singular transformation of Yamada *et al.* (1979) by the relations

$$r = r_0\left(\frac{1-\xi}{2}\right)^{1/2} \quad \text{or} \quad \rho = \frac{r}{r_0} = \left(\frac{1+\xi}{2}\right)^{1/2} \tag{1}$$

$$\theta = \sum_{i=1}^{3} H_i\theta_i \tag{2}$$

where

$$H_1 = \tfrac{1}{2}(\eta-\eta^2), \quad H_2 = 1-\eta^2, \quad H_3 = \tfrac{1}{2}(\eta+\eta^2) \tag{3}$$

and η and ξ are natural coordinates of the element whose ranges are defined as shown in Fig. 2.

The displacement field in the element is assumed to be of the form

$$(\mathbf{u}-\mathbf{u}_0) = \left(\frac{1+\xi}{2}\right)\left[\sum_{i=1}^{3} H_i(\mathbf{u}_i-\mathbf{u}_0)\right], \tag{4}$$

where $\mathbf{u}_0$ and $\mathbf{u}$ represent the three-dimensional displacement vectors of the vertex o and the point P, respectively, and $\mathbf{u}_i$ represents the three-dimensional displacement vector of the ith node ($i = 1, 2, 3$).

In order to simplify the notation and to measure displacements relative to that of the vertex o, we define $\bar{\mathbf{u}}_i = (\mathbf{u}_i-\mathbf{u}_0)$ and $\bar{\mathbf{u}} = (\mathbf{u}-\mathbf{u}_0)$. Using eqn (1), eqn (4) can be written with the new notation as

$$\bar{\mathbf{u}} = \rho^{1/2}\left[\sum_{i=1}^{3} H_i\bar{\mathbf{u}}_i\right]. \tag{5}$$

Since a state of generalized plane strain is considered here for the reasons mentioned

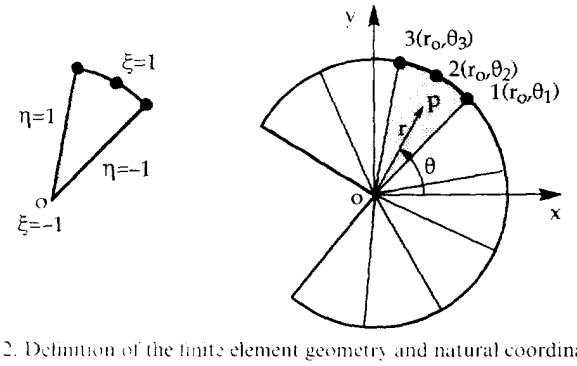

Fig. 2. Definition of the finite element geometry and natural coordinates.

earlier, the displacements are not functions of the coordinate z and $\varepsilon_z = 0$. The remaining strains are obtained directly from eqns (1)–(3) and (5) as

$$\{\boldsymbol{\varepsilon}\} = \begin{Bmatrix} \varepsilon_r \\ \varepsilon_\theta \\ \gamma_{r\theta} \\ \gamma_{rz} \\ \gamma_{\theta z} \end{Bmatrix} = \sum_{i=1}^{3} [\mathbf{B}_i]\{\bar{\mathbf{u}}_i\} = [\mathbf{B}]\{\bar{\mathbf{u}}\}, \quad \{\bar{\mathbf{u}}_i\} = \begin{Bmatrix} \bar{u}_{ri} \\ \bar{u}_{\theta i} \\ \bar{w}_i \end{Bmatrix}, \tag{6}$$

where

$$[\mathbf{B}] = \frac{1}{r_o}\rho^{\lambda-1}(\lambda[\mathbf{B}_a] + [\mathbf{B}_b]),$$

$$[\mathbf{B}_{ia}] = \begin{bmatrix} H_i & 0 & 0 \\ 0 & 0 & 0 \\ 0 & H_i & 0 \\ 0 & 0 & H_i \\ 0 & 0 & 0 \end{bmatrix}, \quad [\mathbf{B}_{ib}] = \begin{bmatrix} 0 & 0 & 0 \\ H_i & \dfrac{2}{\theta_s}\dfrac{\partial H_i}{\partial \eta} & 0 \\ \dfrac{2}{\theta_s}\dfrac{\partial H_i}{\partial \eta} & -H_i & 0 \\ 0 & 0 & 0 \\ 0 & 0 & \dfrac{2}{\theta_s}\dfrac{\partial H_i}{\partial \eta} \end{bmatrix},$$

$$i = 1, 2, 3. \tag{7}$$

To obtain these results, it has been assumed that $\theta_2 = (\theta_1 + \theta_3)/2$, $\theta_s = \theta_3 - \theta_1$, and therefore $\partial\eta/\partial\theta = 2/\theta_s$.

Equations (6) and (7) show that the strains, and therefore the stresses, are proportional to $\rho^{\lambda-1}$. The case where $0 < \mathrm{Re}(\lambda) < 1$ defines a singular stress state at the vertex o of the element. The element depicted in Fig. 2 must satisfy the principal of virtual work in order to be in equilibrium, i.e. in matrix notation,

$$\int_{r_i}^{r_o}\int_{\theta_1}^{\theta_3} (\delta\{\boldsymbol{\varepsilon}\}^{\mathrm{T}}\{\boldsymbol{\sigma}\})tr\,\mathrm{d}r\,\mathrm{d}\theta = r_o\int_{\theta_1}^{\theta_3} (\delta\{\bar{\mathbf{u}}_{ro}\}^{\mathrm{T}}\{\mathbf{T}\})t\,\mathrm{d}\theta, \tag{8}$$

where $\{\boldsymbol{\sigma}\}$ represents the five stresses corresponding to $\{\boldsymbol{\varepsilon}\}$, $\{\mathbf{T}\}$ is the vector of the applied loads T_r, T_θ and T_z at the outer boundary of the element, $\{\bar{\mathbf{u}}_{ro}\}$ represents the displacement vector on the surface $r = r_o$, and t is the thickness of the element. Making use of eqns (1)–(3), eqn (8) can be transformed into

$$\int_{-1}^{1}\int_{-1}^{1} \frac{r_o\rho^{\lambda-1}\theta_s}{4\lambda}(\delta\{\boldsymbol{\varepsilon}\}^{\mathrm{T}}\{\boldsymbol{\sigma}\})tr_o\rho\,\mathrm{d}\xi\,\mathrm{d}\eta = r_o\int_{-1}^{1}\frac{\theta_s}{2}(\delta\{\bar{\mathbf{u}}_{ro}\}^{\mathrm{T}}\{\mathbf{T}\})t\,\mathrm{d}\eta. \tag{9}$$

On the surface $r = r_o$, $\xi = 1$ and therefore we can write, using eqns (1) and (5),

$$\bar{\mathbf{u}}_{ro} = \left[\sum_{i=1}^{3} H_i\bar{\mathbf{u}}_i\right] = [\mathbf{H}]\{\bar{\mathbf{u}}\}. \tag{10}$$

By means of eqns (1) and (10), and knowing that $T_r = \sigma_r$, $T_\theta = \tau_{r\theta}$ and $T_z = \tau_{rz}$ on the surface $r = r_o$, eqn (9) can be rewritten in matrix form as

$$\int_{-1}^{1}\int_{0}^{1}\frac{r_0^2\theta_s}{2}(\delta\{\varepsilon\}^{\mathrm{T}}\{\sigma\})t\rho\,\mathrm{d}\rho\,\mathrm{d}\eta=\frac{r_0\theta_s}{2}\int_{-1}^{1}\delta\{\bar{\mathbf{u}}\}^{\mathrm{T}}[\mathbf{H}]^{\mathrm{T}}\begin{Bmatrix}\sigma_r\\ \tau_{r\theta}\\ \tau_{rz}\end{Bmatrix}t\,\mathrm{d}\eta. \tag{11}$$

In view of eqns (6) and (7), using the constitutive relation $\{\sigma\}=[\mathbf{D}]\{\varepsilon\}$ and integrating with respect to ρ, eqn (11) becomes

$$\frac{\theta_s t}{4\lambda}\delta\{\bar{\mathbf{u}}\}^{\mathrm{T}}\int_{-1}^{1}(\lambda[\mathbf{B}_a]^{\mathrm{T}}+[\mathbf{B}_b]^{\mathrm{T}})[\mathbf{D}](\lambda[\mathbf{B}_a]+[\mathbf{B}_b])\,\mathrm{d}\eta\{\bar{\mathbf{u}}\}$$

$$=\frac{t\theta_s}{2}\delta\{\bar{\mathbf{u}}\}^{\mathrm{T}}\int_{-1}^{1}[\mathbf{H}]^{\mathrm{T}}[\mathbf{d}](\lambda[\mathbf{B}_a]+[\mathbf{B}_b])\,\mathrm{d}\eta\{\bar{\mathbf{u}}\}, \tag{12}$$

where [**d**] is composed of the first, third and fourth rows of matrix [**D**].

Since $\delta\{\bar{\mathbf{u}}\}$ is arbitrary, eqn (12) leads to the following characteristic equation for the entire domain S defined in Fig. 2:

$$(\lambda^2[\mathbf{A}]+\lambda[\mathbf{B}]+[\mathbf{C}])\{\bar{\mathbf{U}}\}=0. \tag{13}$$

where

$$[\mathbf{A}]=\sum_S([\mathbf{k}_a]-[\mathbf{k}_{sa}]),\quad [\mathbf{B}]=\sum_S([\mathbf{k}_b]-[\mathbf{k}_{sb}]),\quad [\mathbf{C}]=\sum_S[\mathbf{k}_c],\quad \{\bar{\mathbf{U}}\}=\sum_S\{\bar{\mathbf{u}}\} \tag{14}$$

$$[\mathbf{k}_a]=\int_{-1}^{1}[\mathbf{B}_a]^{\mathrm{T}}[\mathbf{D}][\mathbf{B}_a]\,\mathrm{d}\eta \tag{15}$$

$$[\mathbf{k}_b]=\int_{-1}^{1}([\mathbf{B}_a]^{\mathrm{T}}[\mathbf{D}][\mathbf{B}_b]+[\mathbf{B}_b]^{\mathrm{T}}[\mathbf{D}][\mathbf{B}_a])\,\mathrm{d}\eta \tag{16}$$

$$[\mathbf{k}_c]=\int_{-1}^{1}[\mathbf{B}_b]^{\mathrm{T}}[\mathbf{D}][\mathbf{B}_b]\,\mathrm{d}\eta \tag{17}$$

$$[\mathbf{k}_{sa}]=2\int_{-1}^{1}[\mathbf{H}]^{\mathrm{T}}[\mathbf{d}][\mathbf{B}_a]\,\mathrm{d}\eta \tag{18}$$

$$[\mathbf{k}_{sb}]=2\int_{-1}^{1}[\mathbf{H}]^{\mathrm{T}}[\mathbf{d}][\mathbf{B}_b]\,\mathrm{d}\eta \tag{19}$$

and where the summation over S implies assembly of the elements into the global model. The matrix [**C**] being singular, the characteristic equation (13) can be transformed in only one way into the standard eigenvalue problem:

$$[\mathbf{S}]\begin{Bmatrix}\bar{\mathbf{V}}\\ \bar{\mathbf{U}}\end{Bmatrix}=\lambda\begin{Bmatrix}\bar{\mathbf{V}}\\ \bar{\mathbf{U}}\end{Bmatrix},\quad [\mathbf{S}]=\begin{bmatrix}\mathbf{0} & \mathbf{I}\\ -\mathbf{A}^{-1}\mathbf{C} & -\mathbf{A}^{-1}\mathbf{B}\end{bmatrix}. \tag{20}$$

Note that [**I**] is the identity matrix of order equal to the number of degrees of freedom of the entire structure, and $\{\bar{\mathbf{V}}\}=(1/\lambda)\times\{\bar{\mathbf{U}}\}$. Admissible values of λ are obtained from eqn (20) and the elements of the eigenvector $\{\bar{\mathbf{U}}\}$ are the normalized nodal values of the displacement in the domain S for each value of λ. Angular variations of the displacements and stresses can be obtained for each element by use of these eigenvectors, eqns (5)–(7) and

the constitutive relation $\{\sigma\} = [\mathbf{D}]\{\varepsilon\}$. If λ is complex, special considerations must be taken in interpreting these angular variations as discussed by Pageau *et al.* (1995b). The 5×5 matrix [**D**] applies to anisotropic materials. The element stiffness matrices [**k**] are evaluated using numerical integration by means of Gaussian quadrature. The matrix [**D**] must be evaluated at each Gauss point during the numerical evaluation of the integrals, such that the anisotropy in the material is correctly taken into consideration. Figure 1 shows the principal axes of orthotropy of the anisotropic material as defined by the 1–2–3 axes, and in which the matrix [**D**] can easily be written. A tensor transformation similar to that used by Pageau and Biggers (1995c) can be used to determine the mechanical properties of this material at the Gauss points in the orientation of the local cylindrical coordinate system defined as the 1′–2′–3′ axes. Note that for isotropic materials, the matrix [**D**] does not depend on the location of the Gauss points, and therefore exact integration can be carried out using three Gauss points. For anisotropic cases, exact integration is not possible and therefore convergence with respect to the number of Gauss points must be evaluated as well as convergence with respect to mesh refinement.

RESULTS

In the following section, the convergence of the values of λ predicted by the finite element code is examined. First, values of λ are predicted for both isotropic and anisotropic materials for the well-known case of a single material with a crack. Finite element results are then compared with known solutions for isotropic and anisotropic multi-material junctions with and without disbonds. Finally, the finite element formulation is applied to an anisotropic, prismatic, three-material junction with material properties that create three-dimensional singular stress and displacement fields.

Convergence of the finite element code

Isotropic materials. As mentioned above, exact integration of the element stiffness matrices is achieved with numerical integration using three Gauss points per element. The question then arises as to the number of elements needed to achieve sufficient accuracy in the evaluations of the root λ obtained from eqn (20). The well-known single-material crack problem shown in Fig. 3 is the first test case used to evaluate convergence. The exact value of λ for this problem is 0.5 for modes I, II and III. The values of λ predicted by the finite

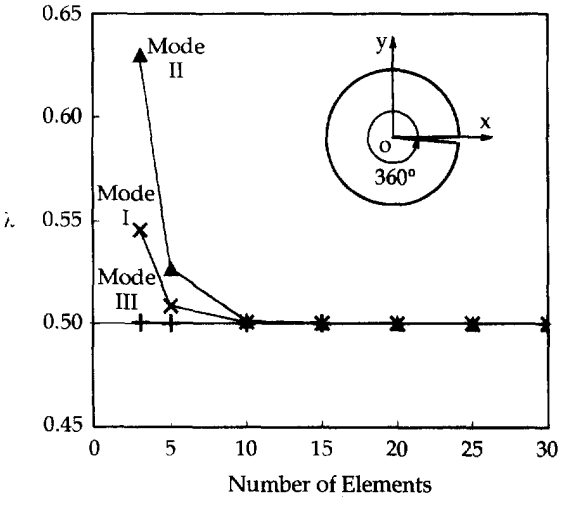

Fig. 3. Convergence of λ for a single isotropic material with a crack (modes I, II and III).

Table 1. Values of λ from the finite element formulation for an isotropic material with a crack (Fig. 3)

Elements in model	Mode I	Mode II	Mode III
3	0.545641	0.630267	0.50039518
5	0.508455	0.526639	0.50005302
10	0.500654	0.501963	0.50000336
15	0.500134	0.500401	0.50000067
20	0.500043	0.500129	0.50000021
25	0.500018	0.500053	0.50000009
30	0.500009	0.500026	0.50000004

element method are shown in Fig. 3 and in Table 1 as a function of the number of equal-sized elements composing the 2π wedge angle. These data show a very strong, monotonic convergence towards the exact solution with four-digit accuracy being achieved with 25 finite elements for modes I and II, and achieved with only five elements for mode III. Note that the results are exactly the same as those obtained for antiplane shear conditions and inplane loads by Pageau *et al.* (1995a,b). This proves that this formulation works well for isotropic cases, and that the generalized plane strain formulation is correct when the inplane and antiplane deformations decouple as is the case here.

Anisotropic materials. With anisotropic materials, Gaussian quadrature does not exactly integrate the element stiffness matrices since the local material properties are not constant over the element. This inexactness adds to the regular problem of convergence associated with element size discussed in the previous section. Instead of using the single material crack problem with a monoclinic material as a test case, here we consider an anisotropic material as shown in Fig. 4 for which the inplane and antiplane deformations are coupled. Indeed, using a monoclinic material would lead to the same uncoupled inplane and antiplane results as those already obtained by Pageau *et al.* (1995a,b). The exact solution for λ is again 0.5 as indicated by Ting and Hoang (1984). The results from eqn (20) are presented in Figs 5–7 and in Table 2. The notation cases I, II and III shown in these three figures and table have been used as opposed to modes I, II and III since the latter notation usually refer to decoupled inplane and out-of-plane crack opening, which is not the case here due to the anisotropy of the material. Here, results for which the eigenvector most closely resembled deformations associated with uncoupled modes I, II and III are referred to as cases I, II and III, respectively. Integration with three, four and five Gauss points per element was used for models with various degrees of mesh refinement. When only a very few elements are used, accuracy is improved for case I and decreased for

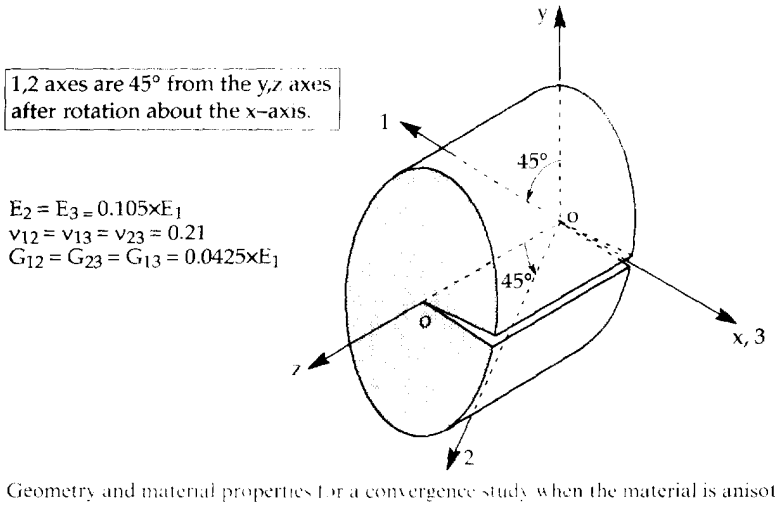

Fig. 4. Geometry and material properties for a convergence study when the material is anisotropic.

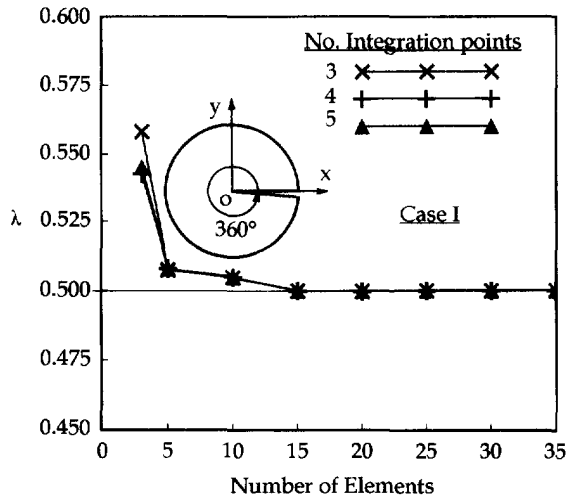

Fig. 5. Convergence of λ for a single anisotropic material with a crack (case I).

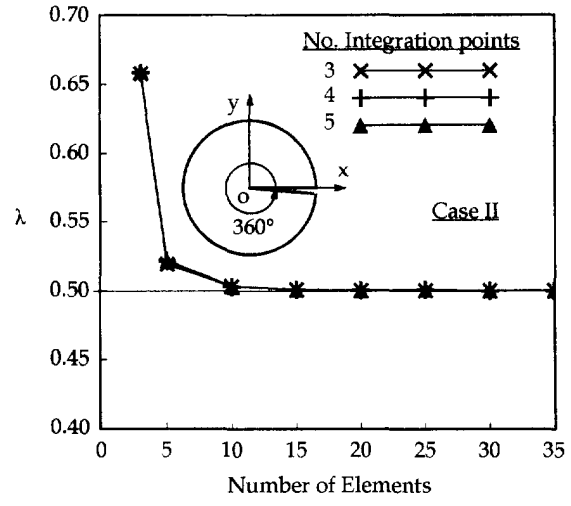

Fig. 6. Convergence of λ for a single anisotropic material with a crack (case II).

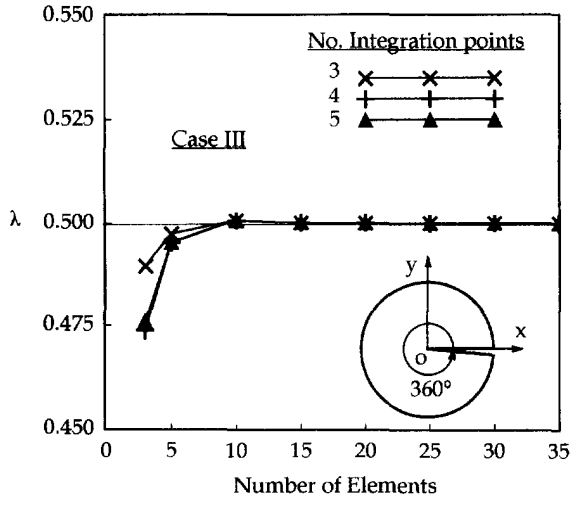

Fig. 7. Convergence of λ for a single anisotropic material with a crack (case III).

Table 2. Values of λ from the finite element formulation for an anisotropic material with a crack (Figs 4–7)

	Case I			Case II			Case III		
Elements in model	3 Gauss points	4 Gauss points	5 Gauss points	3 Gauss points	4 Gauss points	5 Gauss points	3 Gauss points	4 Gauss points	5 Gauss points
3	0.558072	0.542568	0.545006	0.657838	0.658460	0.659116	0.489449	0.473693	0.475947
5	0.507399	0.507927	0.507892	0.519245	0.521751	0.521620	0.497270	0.495183	0.495275
10	0.504604	0.504764	0.504761	0.503018	0.502989	0.502989	0.500667	0.500660	0.500660
15	0.499848	0.499850	0.499850	0.500661	0.500662	0.500662	0.500152	0.500152	0.500152
20	0.499703	0.499702	0.499702	0.500226	0.500227	0.500227	0.500050	0.500050	0.500050
25	0.500021	0.500021	0.500021	0.500083	0.500083	0.500083	0.499998	0.499998	0.499998
30	0.500015	0.500016	0.500016	0.500039	0.500039	0.500039	0.500010	0.500010	0.500010
35	0.500006	0.500006	0.500006	0.500022	0.500022	0.500022	0.499999	0.499999	0.499999

case III as the number of Gauss points in increased. Otherwise, when a reasonable number of elements is used in the model, the integration scheme does not significantly affect the predicted values of λ. Therefore, for computational efficiency, the results to be presented in the remainder of the paper were obtained using three integration points per element. The major difference between the results for the isotropic and anisotropic materials is that in the latter case convergence is oscillatory, especially for case III. In addition, convergence is not as rapid as in the former case. Nevertheless, the results show rapid convergence towards the exact solution with only 20 elements required to give results that are accurate to four digits.

Validation of the finite element code for multi-material wedges

The first case studied, shown in Fig. 8, is a bimaterial wedge composed of two wedge angles, one of angle α, the other of angle β. Both materials are composed of the same fiber/resin composite whose material properties are indicated in Fig. 8. The fiber orientations of the two materials, however, differ from each other and are measured from the y-axis in the y–z plane by the angles θ_1 and θ_2 for materials I and II, respectively. This problem has been solved by Delale (1984) for specific values of the angles θ_1 and θ_2. Using the same values of the angles as Delale (1984), comparative results for the order of the stress singularity can be obtained using Delale's exact formulation based on Lekhnitskii's (1963) theory and the current approximate solution. Results are shown in Tables 3–5. The last column in these tables, and a subsequent table, compares the current value of λ with the analytical value. The percentage error between the numerical and the analytical methods can easily be evaluated as (% error) = ((Current/Analytical) − 1) × 100. As shown by Pageau *et*

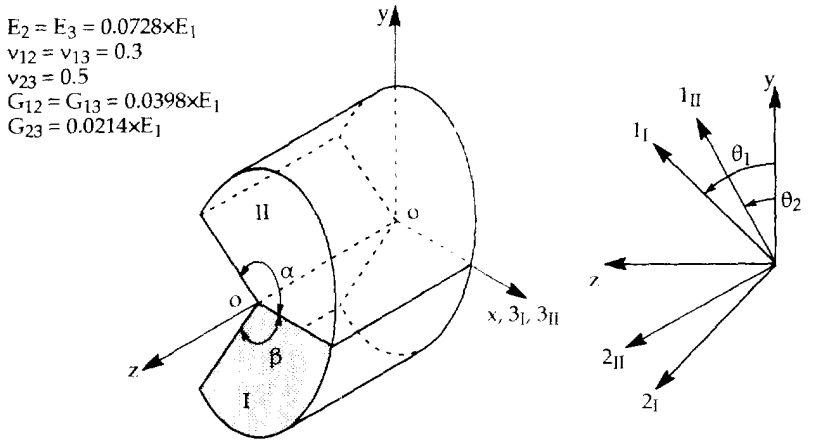

Material I: axis of orthotropy 1_I, 2_I, and 3_I, at an angle θ_1 from the y axis
Material II: axis of orthotropy 1_{II}, 2_{II}, and 3_{II}, at an angle θ_2 from the y axis

Fig. 8. Geometry and material properties of a bi-material wedge.

Table 3. Values of lowest λ for a bi-material wedge with angles $\alpha = \beta = 90$, $\theta_1 = 30$ (Fig. 8)

Angle θ_2	Ten-element model, eqn (20)	Exact value, Delale (1984)	Current λ / Analytical λ
−90	0.9234	Formulation fails	N/A†
−75	0.9270	0.9269	1.0001
−60	0.9419	0.9418	1.0001
−45	0.9612	0.9612	1.0000
−30	0.9744	0.9744	1.0000
−15	0.9768	0.9765	1.0003
0	0.9775	Formulation fails	N/A
15	0.9893	0.9887	1.0006
30	1.0008	formulation fails exact value = 1.0	1.0008
45	0.9837	0.9833	1.0004
60	0.9494	0.9493	1.0001
75	0.9268	0.9267	1.0001
90	0.9234	Formulation fails	N/A

†N/A, not applicable.

Table 4. Values of lowest λ for a bi-material wedge with angles $\alpha = 90$, $\beta = 180$, $\theta_1 = 30$ (Fig. 8)

Angle θ_2	Fifteen-element model, eqn (20)	Exact value, Delale (1984)	Current λ / Analytical λ
−90	0.5818	Formulation fails	N/A†
−75	0.5817	0.5816	1.0002
−60	0.5669	0.5667	1.0003
−45	0.5511	0.5510	1.0002
−30	0.5421	0.5422	0.9998
−15	0.5385	0.5386	0.9998
0	0.5391	Formulation fails	N/A
15	0.5439	0.5441	0.9996
30	0.5527	Formulation fails	N/A
45	0.5645	0.5645	1.0000
60	0.5773	0.5771	1.0003
75	0.5815	0.5813	1.0003
90	0.5818	Formulation fails	N/A

†N/A, not applicable.

Table 5. Values of lowest λ for a bi-material wedge with angles $\beta = 180$, $\theta_1 = 30$, $\theta_2 = 60$ (Fig. 8)

Angle α (deg)	Elements in model	Current FEM,† eqn (20)	Exact value, Delale (1984)	Current λ / Analytical λ
10	19	0.9215	0.9215	1.0000
20	10	0.8543	0.8535	1.0009
30	7	0.7978	0.7950	1.0035
60	8	0.6659	0.6644	1.0023
90	9	0.5777	0.5771	1.0010
120	10	0.5250	0.5257	0.9987
150	11	0.5103	0.5112	0.9982
180	10	0.50119	0.5000	1.0024

† FEM, finite element model.

al. (1995a), it is important for convergence to use elements of equal size to model the bimaterial wedge. As a consequence, all results are given as a function of the number of equal-size elements. For Tables 3 and 4, the number of elements has been chosen such that results are obtained within 0.1% accuracy. For the results in Table 5, the number of elements has been chosen to obtain at least 0.5% accuracy. Note that due to the equal-size element constraint, the number of elements used to obtain the results of Table 5 is a function of the angle α. As a consequence, 19 elements had to be used for the case where $\alpha = 10°$ leading to four-digit accuracy. The results show very good agreement with those obtained

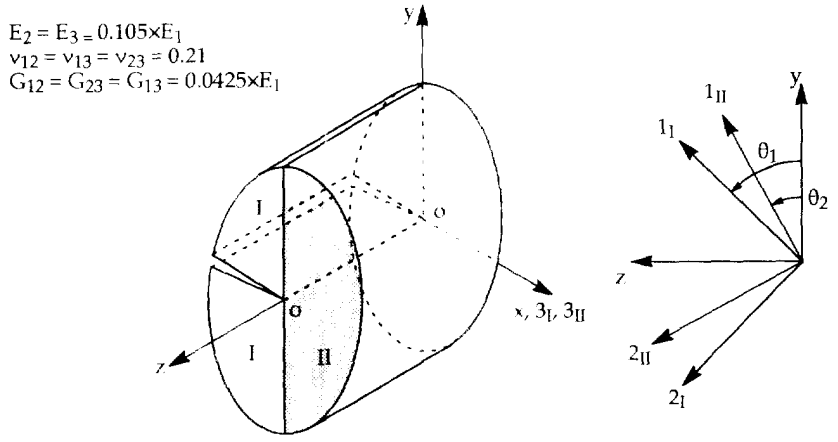

Material I: axis of orthotropy 1_I, 2_I, and 3_I, at an angle θ_1 from the y axis
Material II: axis of orthotropy 1_{II}, 2_{II}, and 3_{II}, at an angle θ_2 from the y axis

Fig. 9. Geometry and material properties for a crack normal to and ending at the interface between two anisotropic materials.

by Delale (1984). Using more elements in the models leads to values closer to the exact values for all cases. Note that only the dominant value λ has been given here (i.e. the value closest to zero) even though some of the secondary values of λ also lead to singular stress states.

The second test case is depicted in Fig. 9. It represents a crack which is normal to and ends at the interface between two anisotropic materials. Both materials are composed of the same fiber resin composite whose material properties are indicated in the figure. The fiber orientations of the two materials, however, differ from each other and are measured from the y-axis in the y–z plane by the angles θ_1 and θ_2 for materials I and II, respectively. This problem has been solved by Ting and Hoang (1984) for numerous values of the angles θ_1 and θ_2. Results are given in Table 6 for selected values of the angles θ_1 and θ_2. They compare well with the results obtained by Ting and Hoang (1984) and convergence to within 0.5% accuracy is achieved with only 20 elements in the model. Here again, increasing the number of elements leads to results which approach those of Ting and Hoang (1984) even closer.

Results for three-material wedges and junctions

Figure 10 depicts the case of a crack at the interface of three materials. Each material is the same fiber resin composite whose local properties are indicated in the figure. The fiber orientations of the three materials, however, differ from each other and are measured

Table 6. Values of singular roots λ_i ($i = 1, 2, 3$) for the interface crack shown in Fig. 9

Angle θ_1, angle θ_2 (deg)	i	Twenty-element model, eqn (20)	Exact value, Ting and Hoang (1984)	Current λ / Analytical λ
45, 60	1	0.442113	0.442364	0.999433
	2	0.499529	0.499327	1.000404
	3	0.522684	0.522684	1.000000
45, −45	1	0.348491	0.348745	0.999272
	2	0.504364	0.504113	1.000498
	3	0.641953	0.642001	0.999925
30, −30	1	0.336894	0.337490	0.998234
	2	0.505549	0.505161	1.000768
	3	0.651883	0.652054	0.999738
90, 0	1	0.500000	0.500000	1.000000
	2	0.511338	0.510962	1.000736
	3	0.658587	0.658892	0.999537

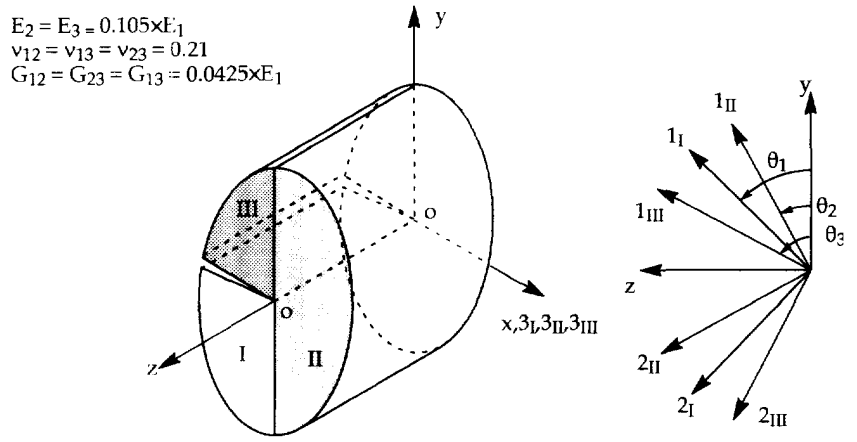

Material I: axis of orthotropy 1_I, 2_I, and 3_I at an angle θ_1 from the y axis
Material II: axis of orthotropy 1_{II}, 2_{II}, and 3_{II} at an angle θ_2 from the y axis
Material III: axis of orthotropy 1_{III}, 2_{III}, and 3_{III} at an angle θ_3 from the y axis

Fig. 10. Geometry and material properties for a crack normal to and ending at the interface between three anisotropic materials.

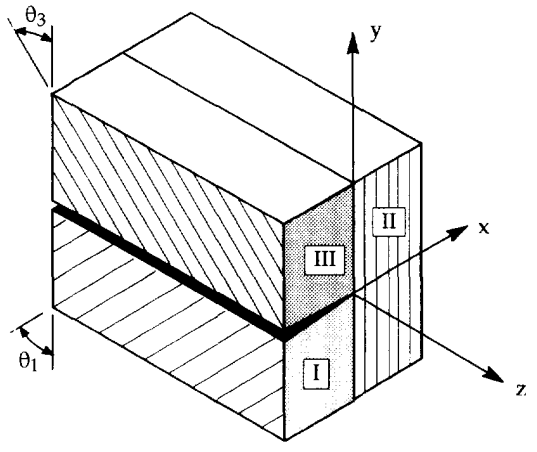

Fig. 11. Schematic of three materials with particular fiber orientations and a crack normal to and ending at the interface.

from the x-axis in the x–z plane by the angles θ_1, θ_2 and θ_3 for materials I, II and III, respectively. This example is provided to show the ease with which the method can be used for complicated material arrangements. For the specific case of $\theta_1 = -\theta_3$ and $\theta_2 = 0°$, for which a schematic representation is shown in Fig. 11, all the eigenvalues of eqn (20) that lead to singular stress states are shown in Table 7 and Fig. 12. These results are obtained within approximately 0.5% accuracy based on the observed convergence trends using a 20-element model. As θ_1 goes to 0°, the well-known modes I, II and III of a crack in a homogeneous orthotropic material are recovered and the three λ values converge to 0.5. Note that the value λ_2 is fairly constant over the entire range studied, whereas λ_1 and λ_3 vary significantly over the same range. The lowest value of λ_1, corresponding to the strongest singularity, occurs for θ_1 approximately equal to 53°. As θ_1 goes to 90°, the three-dimensional deformations of the structure decouple into one-dimensional and two-dimensional deformations as the x–y plane (see Fig. 11) becomes a plane of material symmetry. The eigenvalue λ_2 corresponds to antiplane shear deformation, whereas the other two eigenvalues correspond to inplane deformation.

Figure 13 depicts the case of a three-material junction having materials and geometry as defined in the previous example, except that no crack is present in the current example. The eigenvalues that lead to singular stress states in this case are shown in Table 7 and in

Table 7. Values of all λ between 0 and 1 for the cases depicted in Figs 12 and 13, for the special case $\theta_2 = 0°$, $\theta_1 = -\theta_3$

	With disbond between materials I and III (see Fig. 12)			Without disbond between materials I and III (see Fig. 13)	
$\theta_1 = -\theta_3$	λ_1	λ_2	λ_3	λ_1	λ_2
0	0.498675	0.500000	0.500426	0.999181	1.000007
10	0.483380	0.505698	0.509267	0.979417	0.985042
20	0.453722	0.507514	0.536132	0.942521	0.969417
30	0.420610	0.508612	0.567943	0.913433	0.968623
40	0.393780	0.509514	0.600854	0.908084	0.975970
45	0.384903	0.509910	0.614499	0.915760	0.980782
50	0.379941	0.510264	0.626341	0.929369	0.985588
60	0.384159	0.510826	0.644185	0.965095	0.993672
70	0.411175	0.511178	0.654337	0.991563	0.998373
80	0.461925	0.511326	0.658101	0.999363	0.999852
90	0.500000	0.511338	0.658587	0.999999	1.000681

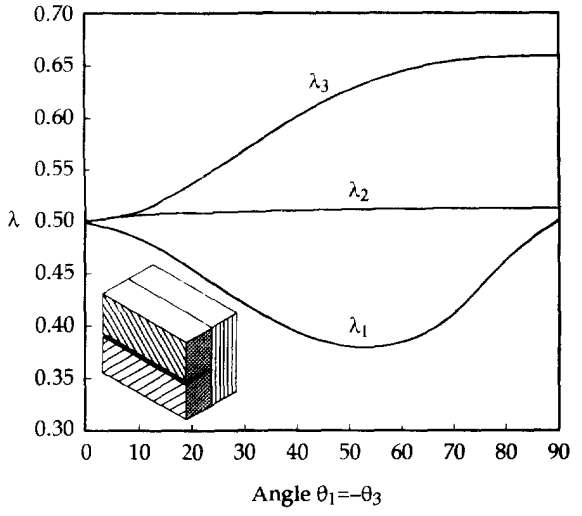

Fig. 12. Values of all λs which lead to singular stress states for the case of Fig. 11 with $\theta_1 = -\theta_3$ and $\theta_2 = 0$.

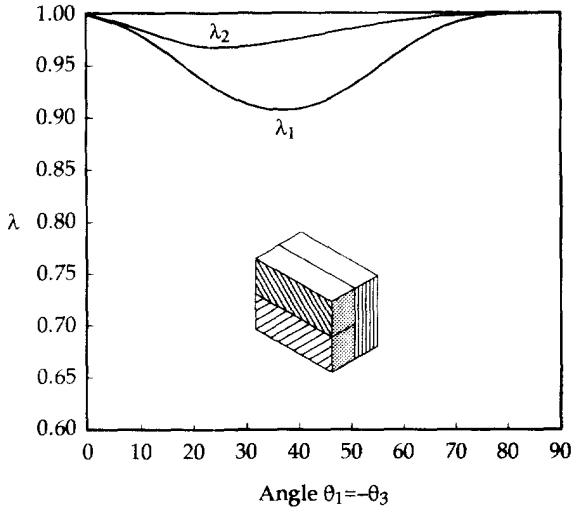

Fig. 13. Values of all λs which lead to singular stress states for the case of Fig. 11 with $\theta_1 = -\theta_3$ and $\theta_2 = 0$, but with no disbond.

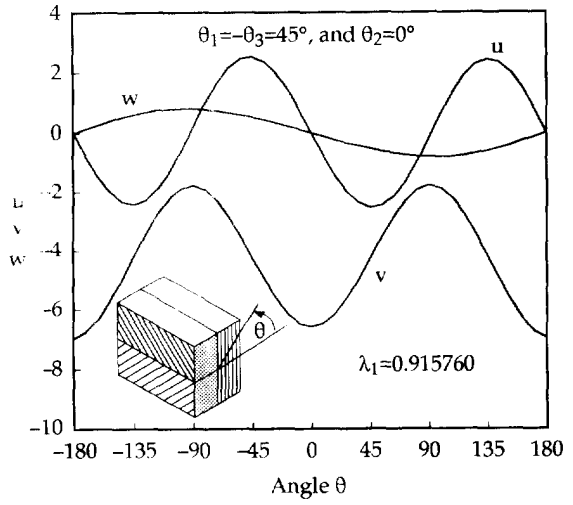

Fig. 14. Three-dimensional displacement fields for the case of Fig. 11 with $\theta_1 = -\theta_3 = 45^\circ$ and $\theta_2 = 0^\circ$ and with no disbond.

Fig. 13. These results are also obtained within approximately 0.5% accuracy using a 20-element model. As θ_1 goes to 0° or 90°, the value of the only two λs which lead to singular stress states converge towards unity since the singular point disappears for these two cases. The variation of λ_1 and λ_2 over the range studied is not as large as for the previous case. The lowest value of λ_1 occurs for θ_1 approximately equal to 37°. Note also that the values of λ for this case are much higher than in the previous case, which shows that the presence of a crack leads to more singular stress states. However, even in the absence of a crack, stress fields with significant singularities exist in the three-material junction. The three-dimensional displacement field corresponding to λ_1 and the eigenvector $\bar{\mathbf{U}}$ from eqn (20) for the case of Fig. 13 with $\theta_1 = -\theta_3 = 45^\circ$ and $\theta_2 = 0^\circ$ is shown in Fig. 14. The three-dimensional stress fields for this problem could easily be obtained following the procedures indicated in previous papers (Pageau *et al.*, 1995a,b) for two-dimensional fields.

Validation of the generalized plane strain assumption

The approach used by Pageau and Biggers (1995c) enables one to obtain the stress and displacement fields at the location where singular stress states occur due to general three-dimensional geometrical discontinuities. In that paper, prismatic multi-material junctions having a locus of singular points that intersects a free surface, or free edge, were considered. There, the finite element model encompasses at most a half-spherical space. Results for the examples considered in the current investigation can be obtained from the general three-dimension formulation at internal singular points if the finite element model encompasses a full spherical space. When results are obtained using the general three-dimensional formulation, no assumption of generalized plane strain condition is made. However, for all cases investigated here, the general three-dimensional formulation gives essentially the same results as the current formulation as long as the values of λ are between 0 and 1. For example, the case shown in Fig. 13 where $\theta_1 = -\theta_3 = 45^\circ$ has two singular roots, $\lambda_1 = 0.913992$ and $\lambda_2 = 0.978030$, according to the general three-dimensional formulation using a model with 128 elements. Both roots are within 0.3% of those obtained with the current formulation and a simple 20-element model. For the corresponding disbonded case shown in Fig. 12 (i.e. $\theta_1 = -\theta_3 = 45^\circ$), the general three-dimensional formulation with a 128-element model leads to three singular roots, $\lambda_1 = 0.381968$, $\lambda_2 = 0.510572$ and $\lambda_3 = 0.614608$. These values agree with those obtained with a 20-element model and the current formulation to within 0.8%. Furthermore, it appears that the results from the 20-element model using the current formulation are superior to those of the larger general three-dimensional model based on the observed convergence trends of the two methods. This comparison validates the conclusion of Ting and Hoang (1984) regarding the effect of assuming generalized plane strain conditions. By assuming generalized plane strain, the current formulation allows one to

simplify the finite element model and to reduce greatly the computational expense in obtaining the asymptotic stress and displacement fields at internal points in structures where the discontinuous geometry is prismatic two-dimensional and the displacement fields are three-dimensional.

CONCLUSIONS

A finite element formulation has been developed for determining the order of the singularity and the angular variation of the displacement and stress fields around a singular point in structures which are prismatic two-dimensional but with three-dimensional displacement fields due to the presence of anisotropic materials. This formulation has the merit of using a simplifying generalized plane strain assumption which has been shown to have no influence on the results compared with a more complicated general three-dimensional formulation. The sectorial element displacement shape functions are quadratic in the angular direction and asymptotic in the radial direction. Numerical integration is required only in the angular direction resulting in a very computationally efficient formulation. The rapid convergence of the formulation has been demonstrated by comparison with several available exact solutions. Low-order quadrature yields very accurate results when a reasonable number of elements is used. Monotonic convergence is observed with mesh refinement in isotropic materials and oscillatory convergence is observed with anisotropic materials. Discrete changes in mechanical properties between adjacent elements cause no difficulty in convergence. Predictions for the order of singularity in multi-material wedges and junctions have been shown to be accurate with very simple models. The angular variation of the singular displacement field corresponding to each root λ is also obtained through solution to the eigenvalue problem. Although all examples presented in this paper had only real roots, the method predicts complex eigenvalues and eigenvectors with equal ease. The accuracy and efficiency shown here suggest that results from this approach could be used to formulate two-dimensional and three-dimensional enriched elements for use in obtaining generalized stress intensity factors in complex geometrical configurations including anisotropic materials.

Acknowledgements—The authors acknowledge the support of NASA Langley Research Center through grant NAG-1-1411 and the computational support of NCSA through grant MSS930014P.

REFERENCES

Delale, F. (1984). Stress singularities in bonded anisotropic materials. *Int. J. Solids Structures* **20,** 31–40.

Eshelby, J. D., Read, W. T. and Shockley, W. (1953). Anisotropic elasticity with application to dislocation theory. *Acta Metall.* **1,** 251–259.

Lekhnitskii, S. G. (1963). *Theory of Elasticity of an Anisotropic Body*. Holden-Day, San Francisco.

Pageau, S. S., Joseph, P. F. and Biggers, S. B. Jr. (1995a). A finite element analysis of the singular stress fields in anisotropic materials loaded in antiplane shear. *Int. J. Numer. Meth. Engng* **38,** 81–97.

Pageau, S. S., Joseph, P. F. and Biggers, S. B. Jr. (1995b). Finite element analysis of anisotropic materials with singular inplane stress fields. *Int. J. Solids Structures* **32,** 571–591.

Pageau, S. S. and Biggers, S. B. Jr. (1995c). Finite element evaluation of free-edge singular stress fields in anisotropic materials. *Int. J. Numer. Meth. Engng*. In press.

Stroh, A. N. (1962). Steady state problems in anisotropic elasticity. *J. Math. Phys.* **41,** 77–103.

Suo, Z. (1990). Singularities, interfaces and cracks in dissimilar anisotropic media. *Proc. R. Soc.* A **427,** 331–358.

Ting, T. C. T. and Hoang, P. H. (1984). Singularities at the tip of a crack normal to the interface of an anisotropic layered composite. *Int. J. Solids Structures* **20,** 439–454.

Yamada, Y., Ezawa, Y., Nishigushi, L. and Okabe, M. (1979). Reconsiderations on singularity or crack tip element. *Int. J. Numer. Meth. Engng* **14,** 1525–1544.

Yamada, Y. and Okumura, H. (1983). Finite element analysis of stress and strain singularity eigenstate in inhomogeneous media or composite materials. In *Hybrid and Mixed Finite Element Methods* (Edited by S. N. Atluri, R. H. Gallagher and O. C. Zienkiewicz), pp. 325–343. Wiley, Chichester.

Zwiers, R. I., Ting, T. C. T. and Spilker, R. L. (1982). On the logarithmic singularity of free-edge stress in laminated composites under uniform extension. *J. Appl. Mech.* **49,** 561–569.